Facile Synthesis of Co_3O_4/$CoF_2 \cdot 4H_2O$/graphene Composites for Supercapacitor Electrodes

Yanhua Li[*], Jinbo Li, Shiying Zhang, Jiaxin Yang

Hunan Province Key Laboratory of Applied Environmental Photocatalysis, Changsha University, Changsha 410022, China
[*]E-mail: liyanhua11@126.com

Co_3O_4/$CoF_2 \cdot 4H_2O$/graphene composites and Co_3O_4/graphene composites are synthesized by a facile microwave-assisted hydrothermal synthesis, followed by calcining at 350 °C. The synthesized composites are characterized by X-ray diffraction, and scanning electron microscopy. Electrochemical property of the prepared composites is measured by cyclic voltammetry and galvanostatic charge-discharge. Results show that Co_3O_4/$CoF_2 \cdot 4H_2O$/graphene composites exhibit better specific capacitance and retention ratio of initial specific capacitance when compared with Co_3O_4/graphene composites. Particularly, Co_3O_4/$CoF_2 \cdot 4H_2O$/graphene composites prepared using $CoSO_4 \cdot 7H_2O$ as material exhibit the highest specific capacitance at various current densities, retention ratio of the specific capacitance at the current density ranging from 1 to 4 A g^{-1} and retention ratio of initial specific capacitance after 1000 cycles, indicating excellent rate capability and cycling stability. These characteristics demonstrate that Co_3O_4/$CoF_2 \cdot 4H_2O$/graphene composites prepared using $CoSO_4 \cdot 7H_2O$ as material possess a great potential application in supercapacitors.

Keywords: Supercapacitors, Co_3O_4, $CoF_2 \cdot 4H_2O$, graphene

1. INTRODUCTION

Recently, supercapacitors in virtue of high power density, rapid charge-discharge capability, and excellent long cycle performance, have been receiving more and more attention. The properties of supercapacitors are mostly decided by the characteristics of electrode materials. Therefore, there are increasing literatures about electrode materials applied as supercapacitors. Electrode materials including but not limited to carbon materials [1-3], transition metal oxides [4-9], transition metal sulfides [10, 11], conducting polymers [12, 13] and their composites [14-16] have been used in supercapacitors. Co_3O_4 as transition metal oxides, due to its high redox activity, low cost, environmental safety and ultrahigh theoretical specific capacitance (3560 F g^{-1}), is a promising

electrode material as supercapacitors. Xiao et al. synthesized 3D hierarchical Co_3O_4 twin-spheres, which exhibits a specific capacitance of 781 F g^{-1} at 0.5 A g^{-1} [17]. Co_3O_4 thin film prepared by a chemical bath deposition method delivers a high specific capacitance of 227 F g^{-1} at 0.2 A g^{-1} [4]. However, Co_3O_4 investigated above possesses the limited capacitance, which is much less than its theoretical specific capacitance. This is because of its low electron conductivity and poor durability in the charge-discharge processes. To overcome these problems, an efficient strategy is introduce carbon materials in Co_3O_4. Graphene, as carbon materials, has been widely used in supercapacitors due to its excellent electronic conductivity, outstanding mechanical flexibility and large surface area [18, 19].

Many approaches are available for synthesizing Co_3O_4/graphene composites for supercapacitors. Park et al. reported that Co_3O_4/graphene composites with carbon blacks filler addition (15 wt.%) delivered a specific capacitance of 341 F g^{-1} at 10 mV s^{-1} [20]. Guan et al. synthesized needle-like Co_3O_4/graphene composites, which showed a specific capacitance of 157.7 F g^{-1} at 0.1 A g^{-1} [19]. We utilized a hydrothermal method to synthesize Co_3O_4/graphene composites, which showed a specific capacitance of 1033.4 F g^{-1} at 0.2 A g^{-1} [21]. Yang et al. synthesized oxygen-vacancy Co_3O_4/graphene composites, which showed remarkable rate capability and long-term cycle stability [14]. However, there are only few reports on the preparation of Co_3O_4/graphene composites by addition of $CoF_2 \cdot 4H_2O$ to increase their performance of supercapacitors.

Herein, we proposed a facile microwave-assisted hydrothermal synthesis to prepare Co_3O_4/$CoF_2 \cdot 4H_2O$/graphene composites for the first time. For comparison, Co_3O_4/graphene composites were synthesized by the same method. More significantly, Co_3O_4/graphene composites were synthesized using $Co(CH_3COO)_2 \cdot 4H_2O$ and graphite oxide as material. However, Co_3O_4/$CoF_2 \cdot 4H_2O$/graphene composites were obtained only using $Co(NO_3)_2 \cdot 6H_2O$ or $CoSO_4 \cdot 7H_2O$ instead of $Co(CH_3COO)_2 \cdot 4H_2O$ under the same condition. Furthermore, complex synthetic routes, which were costly and time consuming, were not involved in the synthesis of Co_3O_4/$CoF_2 \cdot 4H_2O$/graphene composites. Electrochemical studies demonstrated effects of $CoF_2 \cdot 4H_2O$ on capacitive performances of the composites. Results showed that Co_3O_4/$CoF_2 \cdot 4H_2O$/graphene composites exhibited larger specific capacitance than those of Co_3O_4/graphene composites at various current densities. It implied that introducing $CoF_2 \cdot 4H_2O$ in Co_3O_4/graphene composites to obtain Co_3O_4/$CoF_2 \cdot 4H_2O$/graphene composites was an efficient strategy to improve their capacitive performance.

2. EXPERIMENTAL

2.1. Materials Synthesis

Co_3O_4/$CoF_2 \cdot 4H_2O$/graphene composites were prepared by a facile microwave-assisted hydrothermal synthesis. The synthesis process is as follows. 80 mg of graphite oxide was added in 70 mL of deionized water with sonication. Then, 4 mmol of $Co(NO_3)_2 \cdot 6H_2O$ or $CoSO_4 \cdot 7H_2O$, 30 mmol of $CO(NH_2)_2$, and 12 mmol of NH_4F were dissolved into above solution under constant magnetic stirring. Afterwards, the obtained solution was transferred to a double-walled digestion vessel, sealed

and thermally treated at 150 °C for 15 min using a microwave digestion system (MDS-6G, SINEO). After naturally cooling down to room temperature, the obtained precipitates were collected, washed 3 times with deionized water and absolute ethanol, and then dried at 60 °C for 12 h. Finally, the as-prepared powder was calcinated at 350 °C for 3 h to obtain $Co_3O_4/CoF_2 \cdot 4H_2O$/graphene composites. $Co_3O_4/CoF_2 \cdot 4H_2O$/graphene composites synthesized with $Co(NO_3)_2 \cdot 6H_2O$ as material were denoted as $Co_3O_4/CoF_2 \cdot 4H_2O$/G-1. $Co_3O_4/CoF_2 \cdot 4H_2O$/graphene composites prepared with $CoSO_4 \cdot 7H_2O$ as material were referred to as $Co_3O_4/CoF_2 \cdot 4H_2O$/G-2. Co_3O_4/graphene composites, designated as Co_3O_4/G, were synthesized by a microwave-assisted hydrothermal synthesis with 4 mmol of $Co(CH_3COO)_2 \cdot 4H_2O$ instead of 4 mmol of $Co(NO_3)_2 \cdot 6H_2O$ or $CoSO_4 \cdot 7H_2O$ under the same condition.

2.2. Materials Characterization

The structure of as-obtained products was investigated by X-ray diffraction (XRD, Bruker, D8-Advance). The morphology of as-obtained products was observed by scanning electron microscopy (Hitachi SU8000).

2.3. Electrochemical measurements

Electrochemical studies of the as-prepared electrodes were evaluated by cyclic voltammetry (CV), and galvanostatic charge–discharge. All electrochemical measurements were performed on a CHI 660D electrochemical workstation with a three-electrode cell at room temperature. 2 M KOH solution was used as the electrolyte. The working electrode was fabricated as follows. 80 wt % of the as-prepared composites as active material, 15 wt % of acetylene black as conductive agent, and 5 wt % poly(tetrafluoroethylene) as binder were first mixed to form a slurry. Then, the slurry was pasted on a nickel foam substrate (1 cm $\times$ 1 cm) with a spatula and dried naturally. Finally, the electrode was pressed at 10 Mpa and dried at 110 °C for 12 h under vacuum. A Pt plate and a saturated calomel electrode (SCE) were used as the counter and reference electrodes, respectively.

3. RESULTS AND DISCUSSION

3.1. XRD analyses

Fig. 1 shows XRD patterns of Co_3O_4/G, $Co_3O_4/CoF_2 \cdot 4H_2O$/G-1 and $Co_3O_4/CoF_2 \cdot 4H_2O$/G-2. All the peaks in curve 1a can be indexed to Co_3O_4 (JCPDS No. 42-1467) and graphene [21-23]. The characteristic peaks of Co_3O_4 (JCPDS No. 42-1476), $CoF_2 \cdot 4H_2O$ (JCPDS No. 40-0627) and graphene are detected in in curves 1b and 1c. The positions of the XRD peaks in curves 1b and 1c are consistent. However, the peak width at half maxima intensity in curves 1b is larger than that in curves 1c, except for characteristic peak of graphene. According to Scherrer formula [24], the crystallite sizes of Co_3O_4 and $CoF_2 \cdot 4H_2O$ can be estimated. Therefore, the crystallite sizes of Co_3O_4 and $CoF_2 \cdot 4H_2O$ in $Co_3O_4/CoF_2 \cdot 4H_2O$/G-1 synthesized with $Co(NO_3)_2 \cdot 6H_2O$ as material are larger than that of

$Co_3O_4/CoF_2 \cdot 4H_2O/G$-2 prepared with $CoSO_4 \cdot 7H_2O$ as material. These results indicate distinct impact of cobalt salt type on the phase composition and the crystallite sizes of as-synthesized products.
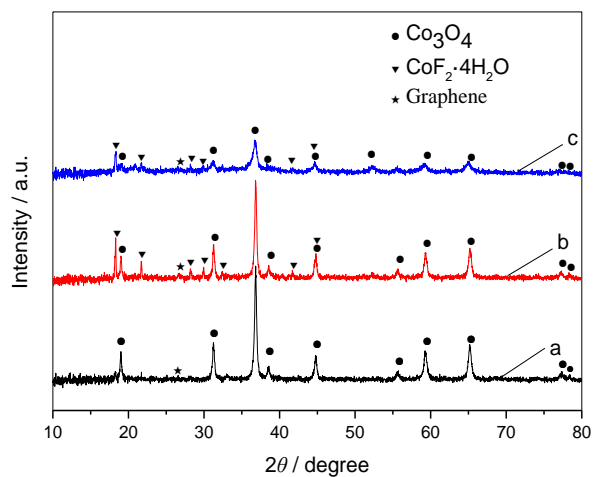
Figure 1. XRD patterns of Co_3O_4/G (a), $Co_3O_4/CoF_2 \cdot 4H_2O/G$-1 (b) and $Co_3O_4/CoF_2 \cdot 4H_2O/G$-2 (c).

3.2. Morphology
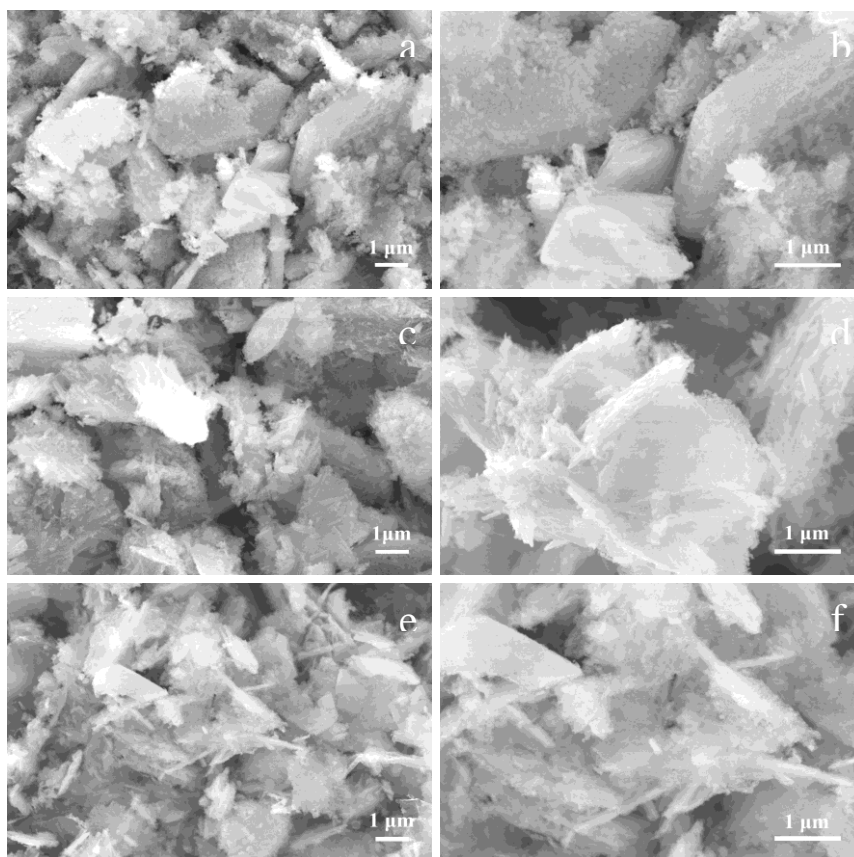
Figure 2. SEM images of Co_3O_4/G (a, b), $Co_3O_4/CoF_2 \cdot 4H_2O/G$-1 (c, d) and $Co_3O_4/CoF_2 \cdot 4H_2O/G$-2 (e, f).

SEM images of Co_3O_4/G, Co_3O_4/CoF_2·$4H_2O$/G-1 and Co_3O_4/CoF_2·$4H_2O$/G-2 are displayed in Fig. 2. For Co_3O_4/G (Fig. 2a and 2b), nanoplates togher with some irregular agglomerates composed of a great of nanoparticles is Co_3O_4 and crumpled structure is graphene. For Co_3O_4/CoF_2·$4H_2O$/G-1 (Fig. 2c-d) and Co_3O_4/CoF_2·$4H_2O$/G-2 (Fig. 2e-f), Co_3O_4 and CoF_2·$4H_2O$ with structure of nanoplates and some irregular agglomerates are observed. Graphene with crumpled structure is also found. However, there are some different morphologies in Co_3O_4/CoF_2·$4H_2O$/G-1 and Co_3O_4/CoF_2·$4H_2O$/G-2. A major difference is that thinner nanoplates exsit in Co_3O_4/CoF_2·$4H_2O$/G-2. Thinner nanoplates can be in favour of the penetration of the electrolyte, leading to improve capacitive properties of material.

3.3. Electrochemical capacitor property

Fig. 3 displays cyclic voltammograms of Co_3O_4/G electrode, Co_3O_4/CoF_2·$4H_2O$/G-1 electrode and Co_3O_4/CoF_2·$4H_2O$/G-2 electrode at a scan rate of 5 mV s^{-1}. The shape of the CV curves exhibits pseudocapacitive behaviour, which originates from Faradaic reactions. Within the potential scanning range, two redox peaks are observed. In Co_3O_4/G electrode, the redox peaks correspond to Faradaic redox reactions as follows [14, 25].

$$CoOOH + OH^- \leftrightarrow CoO_2 + H_2O + e^- \tag{1}$$

$$Co_3O_4 + H_2O + OH^- \leftrightarrow 3CoOOH + e^- \tag{2}$$

However, except for above Faradaic redox reactions, the following reaction exists in Co_3O_4/CoF_2·$4H_2O$/G-1 electrode and Co_3O_4/CoF_2·$4H_2O$/G-2 electrode [26].

$$CoF_2 + 3OH^- \leftrightarrow CoOOH + H_2O + 2F^- + e^- \tag{3}$$
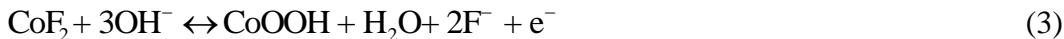
In Co_3O_4/CoF_2·$4H_2O$/G-1 electrode and Co_3O_4/CoF_2·$4H_2O$/G-2 electrode, only two redox peaks rather than three redox peaks are observed. This is because redox reaction (2) and redox reaction (3) are ascribable to Faradaic redox reaction of Co^{2+}/Co^{3+}.
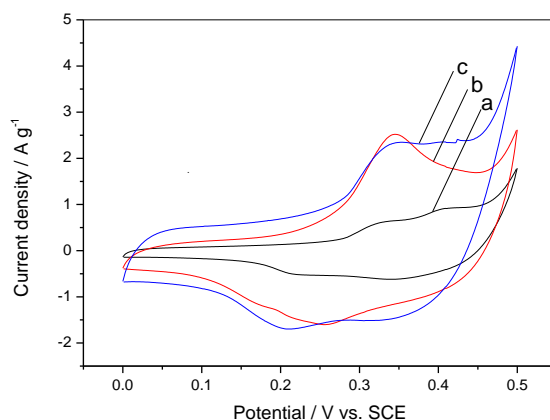
Figure 3. Cyclic voltammograms of Co_3O_4/G electrode (a), Co_3O_4/CoF_2·$4H_2O$/G-1 electrode (b) and Co_3O_4/CoF_2·$4H_2O$/G-2 electrode (c) at a scan rate of 5 mV s^{-1}.

Among three electrodes, the order of the enclosed area of the CV curves ranks from low to high: Co_3O_4/G electrode, Co_3O_4/CoF_2·$4H_2O$/G-1 electrode, Co_3O_4/CoF_2·$4H_2O$/G-2 electrode. As we all know, the specific capacitance is proportional to the enclosed area of the CV curve [24, 27, 28].

Therefore, the specific capacitance of $Co_3O_4/CoF_2 \cdot 4H_2O/G-2$ electrode is the highest, the second is $Co_3O_4/CoF_2 \cdot 4H_2O/G-1$ electrode, and the specific capacitance of Co_3O_4/G electrode is much lower than those of the other two electrodes. This is in agreement with the result of the following charge-discharge measurements. It can be explained as follows. Synergistic effect of Co_3O_4, $CoF_2 \cdot 4H_2O$ and graphene exists in $Co_3O_4/CoF_2 \cdot 4H_2O/G-1$ or $Co_3O_4/CoF_2 \cdot 4H_2O/G-2$ when compared with Co_3O_4/G. Besides, the favorable structure and morphology of $Co_3O_4/CoF_2 \cdot 4H_2O/G-2$ provides better ion accessibility when compared with $Co_3O_4/CoF_2 \cdot 4H_2O/G-1$ and Co_3O_4/G.
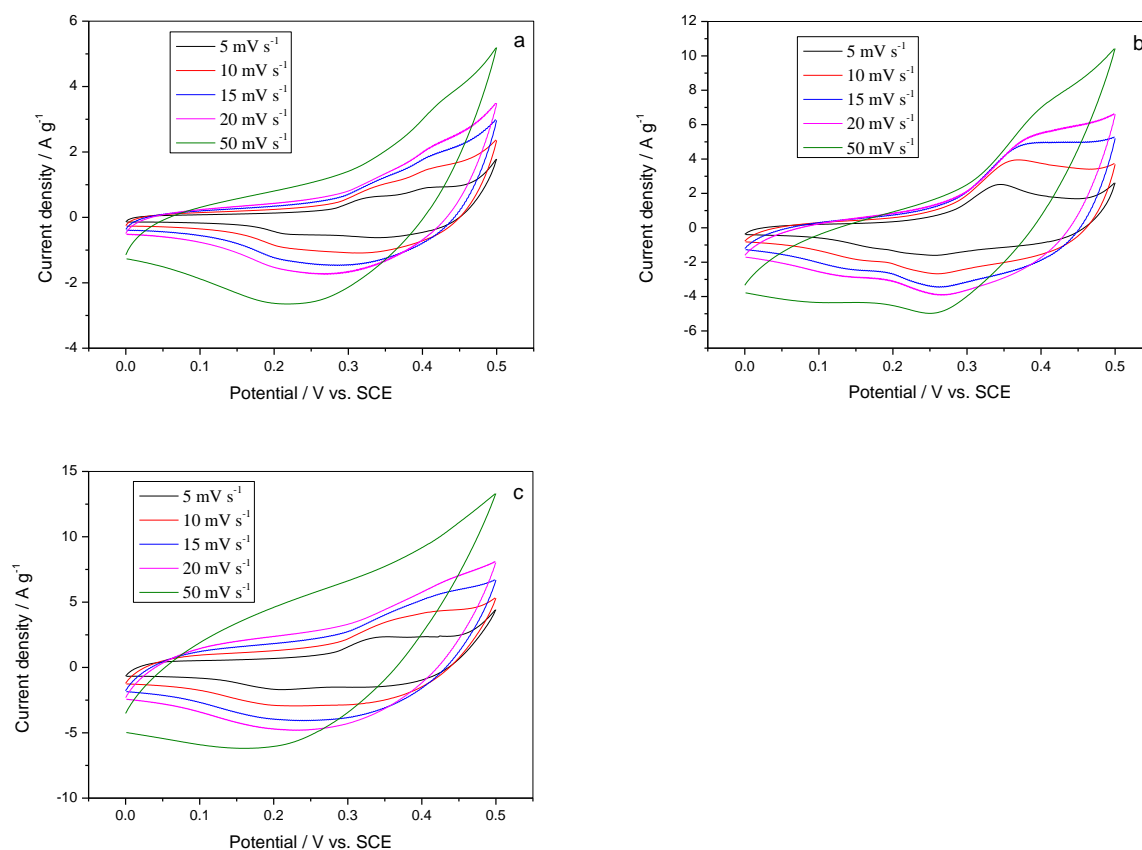
Figure 4. Cyclic voltammograms of Co_3O_4/G electrode (a), $Co_3O_4/CoF_2 \cdot 4H_2O/G-1$ electrode (b) and $Co_3O_4/CoF_2 \cdot 4H_2O/G-2$ electrode (c) in a potential range from -0 to 0.5 V at different scan rates.

Fig. 4 shows cyclic voltammograms Co_3O_4/G electrode, $Co_3O_4/CoF_2 \cdot 4H_2O/G-1$ electrode and $Co_3O_4/CoF_2 \cdot 4H_2O/G-2$ electrode in a potential range from -0 to 0.5 V at scan rates from 5 to 50 mV s^{-1}. The shape of all the curves further signifies the pseudocapacitive behaviour, which corresponds to Faradaic redox reactions of Co^{2+}/Co^{3+} and Co^{3+}/Co^{4+} [29]. Among three electrodes, the peak current density and enclosed area of the CV curves gradually increase with increasing scan rate. Moreover, the anodic peak potential shifts to higher value and the cathodic peak potential shifts to lower value when increasing scan rate, respectively. This can be due to the polarization effect of the electrode.
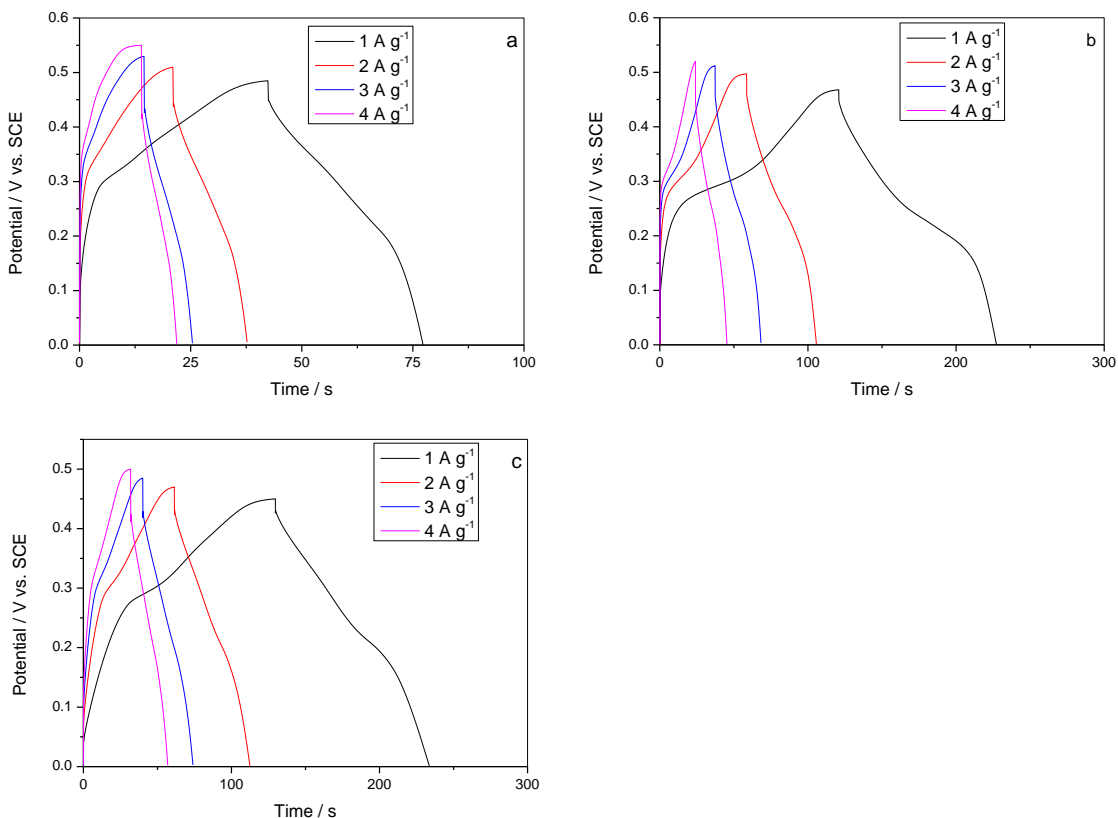
Figure 5. Galvanostatic charge-discharge curves of Co_3O_4/G electrode (a), Co_3O_4/$CoF_2 \cdot 4H_2O$/G-1 electrode (b) and Co_3O_4/$CoF_2 \cdot 4H_2O$/G-2 electrode (c) at different densities.
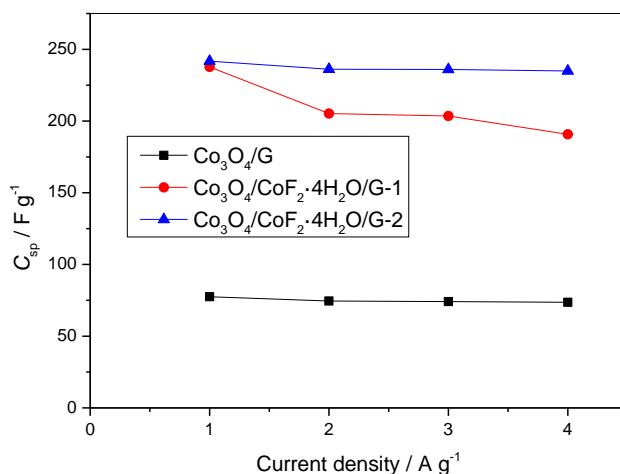
Figure 6. Relationship between the specific capacitance and the current density of Co_3O_4/G electrode, Co_3O_4/$CoF_2 \cdot 4H_2O$/G-1 electrode and Co_3O_4/$CoF_2 \cdot 4H_2O$/G-2 electrode.

Fig. 5 depicts galvanostatic charge–discharge curves of Co_3O_4/G electrode, Co_3O_4/$CoF_2 \cdot 4H_2O$/G-1 electrode and Co_3O_4/$CoF_2 \cdot 4H_2O$/G-2 electrode at the current densities of 1, 2, 3 and 4 A g^{-1}. The shape of the charge-discharge curves shows the characteristics of pseudocapacitance

caused by Faradaic reactions, which substantiates the results of the CV curves. The specific capacitance of the electrode can be calculated from the discharge curves according to the following equation [28, 30-33].

$$C_{sp} = \frac{It}{Vm}$$ (4)

where C_{sp} is the specific capacitance (F g^{-1}), I indicates the discharge current (A), t represents the discharge time (s), V stands for the potential change during discharge, m is the mass of active material, respectively.

Table 1. Comparison of similar electrode materials in literatures with this study.

Materials	Electrolyte	Current density or scan rate	Specific capacitance	Reference
Co_3O_4/graphene	2M KOH	0.1 A g^{-1}	157.7 F g^{-1}	[19]
Co_3O_4/graphene	6M KOH	10 mV s^{-1}	341 F g^{-1}	[20]
Co_3O_4/graphene	2M KOH	0.2 A g^{-1}	1033.4 F g^{-1}	[21]
Co_3O_4/$CoF_2 \cdot 4H_2O$/graphene ($Co(NO_3)_2 \cdot 6H_2O$ as material)	2 M KOH	1 A g^{-1}	237.7 F g^{-1}	This work
Co_3O_4/ $CoF_2 \cdot 4H_2O$/graphene ($CoSO_4 \cdot 7H_2O$ as material)	2 M KOH	1 A g^{-1}	241.8 F g^{-1}	This work

Based on the equation (4), the specific capacitance of Co_3O_4/G electrode, Co_3O_4/$CoF_2 \cdot 4H_2O$/G-1 electrode and Co_3O_4/$CoF_2 \cdot 4H_2O$/G-2 electrode at different current densities is shown in Fig. 6. The specific capacitance of three electrodes follows the following descending order: Co_3O_4/$CoF_2 \cdot 4H_2O$/G-2 electrode, Co_3O_4/$CoF_2 \cdot 4H_2O$/G-1 electrode, Co_3O_4/G electrode. This is in accordance with the CV results. The specific capacitance of Co_3O_4/G electrode, Co_3O_4/$CoF_2 \cdot 4H_2O$/G-1 electrode and Co_3O_4/$CoF_2 \cdot 4H_2O$/G-2 electrode at 1 A g^{-1} are 77.5, 237.7 and 241.8 F g^{-1}, respectively. Compared with Co_3O_4/G electrode, the specific capacitance of Co_3O_4/$CoF_2 \cdot 4H_2O$/G-1 electrode and Co_3O_4/$CoF_2 \cdot 4H_2O$/G-2 electrode at 1 A g^{-1} is 3.07 times and 3.12 times, respectively. This manifests that Co_3O_4/graphene composites by addition of $CoF_2 \cdot 4H_2O$ can greatly enhance their performance of supercapacitors. The reason for this has been explained in analyzing the specific capacitance according to the CV curves. A comparison of similar electrode materials in literatures with this study was shown in Table 1. The specific capacitance values of Co_3O_4/$CoF_2 \cdot 4H_2O$/G-1 electrode (237.7 F g^{-1} at 1 A g^{-1}) and Co_3O_4/ $CoF_2 \cdot 4H_2O$/G-2 electrode (241.8 F g^{-1} at 1 A g^{-1}) are much higher than that of reported Co_3O_4/graphene composite electrode (157.7 F g^{-1} at 0.1 A g^{-1}) [19]. They are not as high as those of Co_3O_4/graphene composite electrode [20, 21]. However, in this work, Co_3O_4/$CoF_2 \cdot 4H_2O$/G-1 and Co_3O_4/$CoF_2 \cdot 4H_2O$/G-2 are synthesized with microwave-assisted hydrothermal synthesis, which were a short consuming-time (15 min). Besides, this work provides a method to enhance the specific capacitance of transition metal oxides/graphene composite. When the

current density increases to 4 A g^{-1}, Co$_3$O$_4$/G electrode, Co$_3$O$_4$/CoF$_2$·4H$_2$O/G-1 electrode and Co$_3$O$_4$/CoF$_2$·4H$_2$O/G-2 electrode show a specific capacitance retention of 95.0%, 80.2% and 97.1%, respectively. It implies that Co$_3$O$_4$/CoF$_2$·4H$_2$O/graphene composites prepared with CoSO$_4$·7H$_2$O as material exhibits excellent rate capability. Although the retention ratios of the specific capacitance for Co$_3$O$_4$/CoF$_2$·4H$_2$O/G-1 electrode is the lowest, the specific capacitance of Co$_3$O$_4$/CoF$_2$·4H$_2$O/G-1 electrode at 4 A g^{-1} is 2.59 times higher than that of Co$_3$O$_4$/G electrode.

The cycling stability of Co$_3$O$_4$/G electrode, Co$_3$O$_4$/CoF$_2$·4H$_2$O/G-1 electrode and Co$_3$O$_4$/CoF$_2$·4H$_2$O/G-2 electrode is evaluated by galvanostatic charge–discharge tests at the current density of 1 A g^{-1} and the results are shown in Figure 7. After 1000 cycles, the specific capacitance retention of Co$_3$O$_4$/G electrode, Co$_3$O$_4$/CoF$_2$·4H$_2$O/G-1 electrode and Co$_3$O$_4$/CoF$_2$·4H$_2$O/G-2 electrode is 91.5%, 94.6% and 95.2%, respectively. It indicates that Co$_3$O$_4$/CoF$_2$·4H$_2$O/G-1 electrode and Co$_3$O$_4$/CoF$_2$·4H$_2$O/G-2 electrode show better cycling stability than Co$_3$O$_4$/G electrode. The specific capacitance retention of Co$_3$O$_4$/CoF$_2$·4H$_2$O/G-1 electrode and Co$_3$O$_4$/CoF$_2$·4H$_2$O/G-2 electrode higher than that of previously reported Co$_3$O$_4$/graphene electrode [19-21].
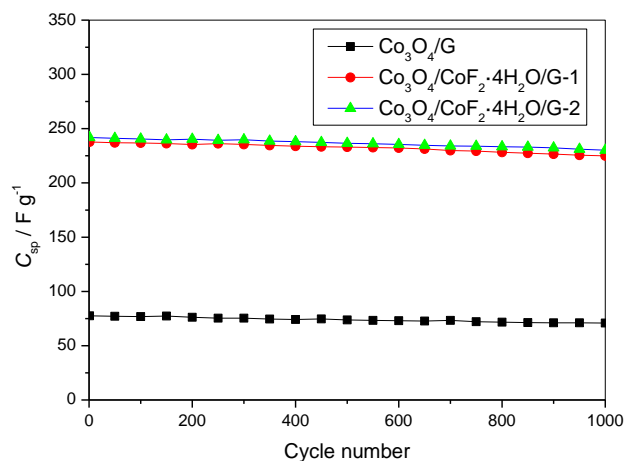
Figure 7. Cycling performance of Co$_3$O$_4$/G electrode, Co$_3$O$_4$/CoF$_2$·4H$_2$O/G-1 electrode and Co$_3$O$_4$/CoF$_2$·4H$_2$O/G-2 electrode at the current density of 1 A g^{-1}.

4. CONCLUSIONS

A microwave-assisted hydrothermal has been successfully developed for the synthesis of Co$_3$O$_4$/CoF$_2$·4H$_2$O/graphene composites and Co$_3$O$_4$/graphene composites. The specific capacitance of composites ranks from high to low as follows: Co$_3$O$_4$/CoF$_2$·4H$_2$O/graphene composites obtained using CoSO$_4$·7H$_2$O as material, Co$_3$O$_4$/CoF$_2$·4H$_2$O/graphene composites obtained using Co(NO$_3$)$_2$·6H$_2$O as material, Co$_3$O$_4$/graphene composites. Among three composites, Co$_3$O$_4$/CoF$_2$·4H$_2$O/graphene composites prepared using CoSO$_4$·7H$_2$O as material exhibit high specific capacitance (241.8 F g^{-1} at 1 A g^{-1}), retention ratio of the specific capacitance (97.1% at the current density ranging from 1 to 4 A g^{-1}) and an excellent cycling stability (95.2% retention after 1000 cycles), indicating excellent rate

capability and cycling stability. These characteristics demonstrate that $Co_3O_4/CoF_2 \cdot 4H_2O$/graphene composites prepared using $CoSO_4 \cdot 7H_2O$ as material possess a great potential application in supercapacitors.

References

1. Q. Wang, J. Yan and Z.J. Fan, *Energy Environ. Sci.*, 9 (2016) 729.
2. Y.F. Song, J. Yang, K. Wang, S. Haller, Y.G. Wang, C.X. Wang and Y.Y. Xia, *Carbon*, 96 (2016) 955.
3. F. Bonaccorso, L. Colombo, G. Yu, M. Stoller, V. Tozzini, A.C. Ferrari, R.S. Ruoff and V. Pellegrini, *Science*, 347 (2015) 1246501.
4. Y.H. Li, K.L. Huang, Z.F. Yao, S.Q. Liu and X.X. Qing, *Electrochim. Acta*, 56 (2011) 2140.
5. S. Bag and C.R. Raj, *J. Mater. Chem. A*, 4 (2016) 587.
6. Y.B. Zhang and Z.G. Guo, *Chem. Commun.*, 50 (2014) 3443.
7. H.S. Kim, J.B. Cook, H. Lin, J.S. Ko, S.H. Tolbert, V. Ozolins and B. Dunn, *Nat. Mater.*, 16 (2017) 454.
8. M. Zheng, X. Xiao, L. Li, P. Gu, X. Dai, H. Tang, Q. Hu, H. Xue and H. Pang, *Science China-Materials*, 61 (2018) 185.
9. Y. Wang, X. Xiao, H. Xue and H. Pang, *Chemistryselect*, 3 (2018) 550.
10. H.P. Zhou, Y.J. Cao, Z.L. Ma and S.L. Li, *Nanotechnology*, 29 (2018) 195201.
11. X.M. Geng, Y.L. Zhang, Y. Han, J.X. Li, L. Yang, M. Benamara, L. Chen and H.L. Zhu, *Nano Lett.*, 17 (2017) 1825.
12. H.H. Zhou and X.M. Zhi, *Mater. Lett.*, 221 (2018) 309.
13. Q.F. Meng, K.F. Cai, Y.X. Chen and L.D. Chen, *Nano Energy*, 36 (2017) 268.
14. S.H. Yang, Y.Y. Liu, Y.F. Hao, X.P. Yang, W.A. Goddard, X.L. Zhang and B.Q. Cao, *Advanced Science*, 5 (2018) 1700659.
15. Y. Song, T.Y. Liu, B. Yao, T.Y. Kou, D.Y. Feng, X.X. Liu and Y. Li, *Small*, DOI 10.1002/smll.201700067(2017) 1700067
16. R. Kumar, R.K. Singh, A.R. Vaz, R. Savu and S.A. Moshkalev, *ACS Appl. Mater. Interfaces*, 9 (2017) 8880.
17. Y. Xiao, S. Liu, F. Li, A. Zhang, J. Zhao, S. Fang and D. Jia, *Adv. Funct. Mater.*, 22 (2012) 4052.
18. M.F. El-Kady, V. Strong, S. Dubin and R.B. Kaner, *Science*, 335 (2012) 1326.
19. Q. Guan, J.L. Cheng, B. Wang, W. Ni, G.F. Gu, X.D. Li, L. Huang, G.C. Yang and F.D. Nie, *ACS Appl. Mater. Interfaces*, 6 (2014) 7626.
20. S. Park and S. Kim, *Electrochim. Acta*, 89 (2013) 516.
21. Y.H. Li, S.Y. Zhang, Q.Y. Chen and J.B. Jiang, *Int. J. Electrochem. Sci.*, 10 (2015) 6199.
22. D.H. Zhang and W.B. Zou, *Curr. Appl. Phys.*, 13 (2013) 1796.
23. Y.H. Li, J.B. Li, S.Y. Zhang, N.F. Wang and Z. Zhou, *Int. J. Electrochem. Sci.*, 10 (2015) 8005.
24. Y.R. Zhu, X.B. Ji, Z.P. Wu, W.X. Song, H.S. Hou, Z.B. Wu, X. He, Q.Y. Chen and C.E. Banks, *J. Power Sources*, 267 (2014) 888.
25. M. Zhou, F. Lu, X.S. Shen, W.W. Xia, H. He and X.H. Zeng, *J. Mater. Chem. A*, 3 (2015) 21201.
26. R. Ma, Y. Zhou, L. Yao, G. Liu, Z. Zhou, J.-M. Lee, J. Wang and Q. Liu, *J. Power Sources*, 303

(2016) 49.
27. Y. Li, X. Peng, J. Xiang and J. Yang, *Int. J. Electrochem. Sci.*, 12 (2017) 10763.
28. Y. Li and X. Peng, *ChemistrySelect*, 2 (2017) 8959.
29. S.H. Yue, H. Tong, L. Lu, W.W. Tang, W.L. Bai, F.Q. Jin, Q.W. Han, J.P. He, J. Liu and X.G. Zhang, *J. Mater. Chem. A*, 5 (2017) 689.
30. Y.H. Li, K.L. Huang, D.M. Zeng, S.Q. Liu and Z.F. Yao, *J. Solid State Electrochem.*, 14 (2010) 1205.
31. X. Yu, B. Lu and Z. Xu, *Adv. Mater.*, 26 (2014) 1044.
32. Y.H. Li, K.L. Huang, S.Q. Liu, Z.F. Yao and S.X. Zhuang, *J. Solid State Electrochem.*, 15 (2011) 587.
33. Y.H. Li and Q.Y. Chen, *Asian J. Chem.*, 24 (2012) 4736.